Atomic Force Microscopy and Electron Microscopy Analysis of Retrovirus Gag Proteins Assembled in Vitro on Lipid Bilayers

Guy Zuber and Eric Barklis
Vollum Institute and Department of Microbiology, Oregon Health Sciences University, Portland, Oregon 97201-3098 USA

ABSTRACT We have used an in vitro system that mimics the assembly of immature Moloney murine leukemia virus (M-MuLV) particles to examine how viral structural (Gag) proteins oligomerize at membrane interfaces. Ordered arrays of histidine-tagged Moloney capsid protein (his-MoCA) were obtained on membrane bilayers composed of phosphatidylcholine (PC) and the nickel-chelating lipid 1,2-di-*O*-hexadecyl-sn-glycero-3-(1′-2″-R-hydroxy-3′*N*-(5-amino-1-carboxypentyl)imino-diacetic acid)propyl ether (DHGN). The membrane-bound arrays were analyzed by electron microscopy (EM) and atomic force microscopy (AFM). Two-dimensional projection images obtained by EM showed that bilayer-bound his-MoCA proteins formed cages surrounding different types of protein-free cage holes with similar cage holes spaced at 81.5-Å distances and distances between dissimilar cage holes of 45.5 Å. AFM images, showing topological features viewed near the membrane-proximal domain of the his-MoCA protein, revealed a cage network of only symmetrical hexamers spaced at 79-Å distances. These results are consistent with a model in which dimers constitute structural building blocks and where membrane-proximal and distal his-MoCA regions interact with different partners in membrane-bound arrays.

INTRODUCTION

C-type retroviruses, such as the Moloney murine leukemia virus (M-MuLV), represent a family of RNA viruses that replicate through a DNA intermediate (Coffin et al., 1997). They are composed of cellular and viral components and are enveloped by host-derived lipid membranes that contain proteins encoded by retroviral *env* genes. The virus core is composed of 1000–5000 copies of the viral Gag proteins; 10–100 copies of *pol* gene-encoded proteins, which include the viral protease, reverse transcriptase, RNAse H, and integrase; two copies of the viral RNA genome; and cellularly derived tRNAs that serve as primers during reverse transcription (Coffin et al., 1997). The assembly of C-type retrovirus particles appears to occur at the plasma membranes of infected cells and is directed by the Gag protein, which has been shown to be necessary and sufficient for particle assembly. Most mammalian retrovirus Gag proteins are synthesized as precursor polyproteins (Pr^{Gag}) and normally are cleaved into the mature processed Gag proteins by the viral protease (PR) during or after budding. Processing of Pr^{Gag} results in a major morphological change in virus particles, in which electron-dense material adjacent to the periphery of the immature virion reorganizes into the central and dense superstructure of the mature virus. For M-MuLV, processing of Pr^{Gag} yields the four mature Gag proteins, matrix (MA), p12, capsid (CA), and nucleocapsid (NC). While each mature Gag protein serves an essential function for replication, several Gag domains are dispensable with regard to virus particle assembly. For instance, deletion of p12 has been shown to be compatible with particle assembly (Hansen and Barklis, 1995). Moreover, the only part of MA necessary for HIV or M-MuLV assembly appears to be its membrane-binding myristate anchor (Wang et al., 1993; Faecke et al., 1993; Barklis et al., 1997). Furthermore, while the RNA-binding retrovirus NC domains contribute to the efficiency of particle formation (Campbell and Vogt, 1995; Wills et al., 1994), under some circumstances they can be replaced in vivo (Zhang et al., 1995), and they are not essential to the formation of particle-like structures in vitro (Gross et al., 1998; Von Schwedler et al., 1998). This leaves the capsid, or a portion of the CA domain, as central to the particle production process.

Although some Gag protein functions seem to be well defined, the three-dimensional structures of retroviruses are not. A major obstacle has been the heterogeneity of naturally occurring virus particles. Nevertheless, researchers have determined the structures of some Gag protein domains and their derivatives (Gitti et al., 1996; Gamble et al., 1996; Hill et al., 1996; DeGuzman et al., 1998; Dememe et al., 1994; Fass et al., 1997), and certain Gag domains can assemble into rod- or sphere-shaped structures in vitro (Campbell and Vogt, 1995; Von Schwedler et al., 1998; Gross et al., 1998). However, to understand the mechanism of C-type retrovirus assembly, it is important to analyze how Gag proteins organize on membranes, where virus particle assembly occurs (Coffin et al., 1997). One such analysis was an electron microscopy (EM) study of HIV Pr^{Gag} proteins assembled at the plasma membranes of baculovirus vector-infected cells (Nermut et al., 1994). At low resolution (40–50 Å), the Pr^{Gag} proteins appeared to form cage-like structures beneath the membranes. In an effort to improve upon Gag-membrane structure studies, we recently devised an in vitro method for the analysis of Gag-membrane interactions (Barklis et al., 1997, 1998). The approach, which is based on previous lipid monolayer studies (Darst et al., 1991; Uzgiris and Kornberg, 1983), employs

Received for publication 10 November 1998 and in final form 20 September 1999.

Address reprint requests to Dr. Eric Barklis, Vollum Institute and Department of Microbiology, Oregon Health Sciences University, 3181 S.W. Sam Jackson Park Road, Portland, OR 97201-3098. Tel.: 503-494-8098; Fax: 503-494-6862; E-mail: barklis@ohsu.edu.

0006-3495/00/01/373/12 $2.00

histidine-tagged (his-tagged) Gag protein derivatives and a model membrane consisting of egg phosphatidylcholine (PC) and the novel nickel-chelating lipid 1,2-di-*O*-hexadecyl-*sn*-glycero-3-(1′-2″-R-hydroxy-3′-*N*-(5-amino-1-carboxypentaiminodiacetic acid) (DHGN) (see Fig. 1; Barklis et al., 1997). Using this system to produce samples for EM analysis, we have found that membrane-bound HIV-1 capsid proteins formed hexamer-trimer cages (Barklis et al., 1998) consistent with previous lower resolution studies (Nermut et al., 1994), while M-MuLV capsid proteins formed distinct hexamer-hexamer cages (Barklis et al., 1997). To extend these results, we have adapted our procedures to permit the imaging of lipid bilayer-bound M-MuLV his-tagged capsid proteins (his MoCA) by both EM and atomic force microscopy (AFM) in buffer solution (Binnig et al., 1986; Hansma and Hoh, 1994; Muller et al., 1995; Shao and Yang, 1995; Brown et al., 1998; Czajkowsky et al., 1998; Fotiadis et al., 1998; Sato et al., 1998). In agreement with monolayer findings, our EM projections show that bilayer-bound his-MoCA forms a protein cage surrounding different types of cage holes, in which similar cage holes are spaced at 81.5-Å intervals, while dissimilar holes occur every 45–46 Å. AFM images, showing topological features, revealed a cage network of only symmetrical hexamers spaced at 79-Å distances. Our results are consistent with a model in which dimers constitute structural building blocks and where membrane-proximal and distal his-MoCA regions interact with different partners in membrane-bound arrays.

MATERIALS AND METHODS

Materials

Egg phosphatidylcholine (PC) was purchased from Avanti Polar Lipids. DHGN was prepared by D. Thompson and charged with nickel as described (Barklis et al., 1997). Highly oriented pyrolytic graphite (HOPG) and mica AFM substrates were from Digital Instruments (Santa Barbara, CA) and Ted Pella, respectively, and carbon EM grids (300 mesh) were from Ted Pella. Water was filtered with a MilliQ purification system.

Construction of the vector for bacterial expression of M-MuLV capsid protein

A M-MuLV capsid-coding region cassette was inserted into the *Bam*HI site of pET15B (Novagen). The cassette was constructed by polymerase chain reaction, generating a *Bam*HI site at the amino-terminus of the CA-coding region, and adding a *Bam*HI linker at the carboxy-terminal *Msc*I site of this region. The respective N- and C-terminal ends of the cassette are GGAT/**C**CC, where the bold C is the M-MuLV viral nucleotide 1266 and TTG/**G**CGGATCC, where the bold G is viral nucleotide 2055. The plasmid pET15B-MoCA then was introduced into *Escherichia coli* strain BL21(DE3)/pLys S (Novagen), and the bacteria was stored at −80°C in 50% glycerol.

Protein expression and purification

Cells of *E. coli* strain BL21(DE3)/pLys S containing pET15B-MoCA were grown at 37°C in LB plus 15 mg/L chloramphenicol and 50 mg/L ampicillin to an OD600 of 0.7. Protein expression then was induced by the addition of isopropyl-β-D-thiogalactopyranoside (IPTG) 0.5 mM, and after 3 h of shaking at room temperature the bacteria were harvested by centrifugation and stored at −80°C. For purification, frozen bacterial pellets were resuspended in lysis buffer (50 mM sodium phosphate, pH 7.8, 300 mM NaCl, 1 mM phenylmethylsulfonyl fluoride, 2 mM β-mercaptoethanol) and disrupted in a French press. Cellular debris was removed by centrifugation (12,000 × *g*; 15 min; 4°C), and his-MoCA proteins were purified by two cycles of nondenaturing affinity nickel-chelate chromatography, using a stepwise gradient of imidazole (0, 10, and 250 mM in 50 mM sodium phosphate, 10% glycerol, 0.5 M NaCl, pH 7.8 for washes, pH 6.0 for elutions). Fraction purities were assessed by a combination of Coomassie staining and immunoblotting of electrophoretically separated proteins. Once identified, pure fractions were desalted on Sephadex G-25 spin columns equilibrated with 5 mM 3-(*N*-morpholino)propanesulfonic acid (MOPS) (pH 7.8), 10% glycerol, and proteins were stored at −80°C.

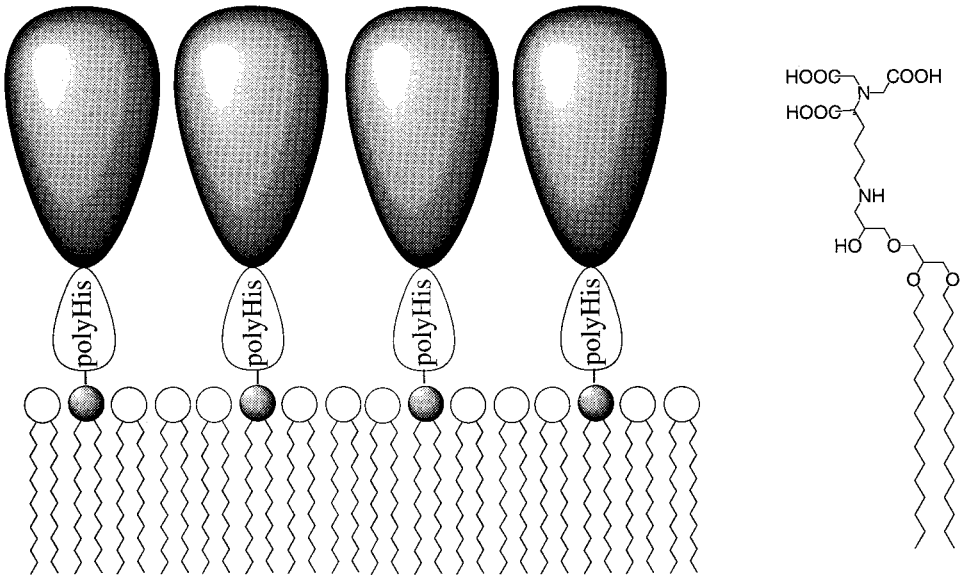

FIGURE 1 Assembly of his-tagged proteins on lipid membranes. Shown is a schematic view of the system used for forming histidine-tagged protein arrays on a monolayer of nickel chelating lipid and phosphatidyl choline at an interface. The structure of DHGN, our nickel-chelating lipid, is shown on the right. For analysis of monolayers by EM, arrays are lifted onto EM grids, stained or frozen in vitrous water, and viewed. For examination of bilayer-bound proteins, liposomes with bound proteins are transferred to EM grids or AFM substrates for viewing.

Preparation of vesicles containing Ni^{2+}-DHGN

Ni^{2+}-DHGN (10 nmol) and egg phosphatidylcholine (100 nmol) in chloroform solutions were mixed and dried under a flux of nitrogen. The lipids then were fully dried under vacuum and resuspended to 50 μM Ni^{2+}-DHGN and μM PC in 2× PNG buffer (200 μl) by sonication in an ultrasonic bath for 10 min. Vesicles were stored at 0–4°C for up to 2 weeks. Alternatively, and with similar success, vesicles were prepared in 10 mM MOPS buffer (pH 7.8), 50 mM NaCl, by detergent dialysis techniques (Tauskela et al., 1992).

Specimen preparation

The his-MoCA proteins (5 μl, 1–5 μg) were mixed gently with 5-μl vesicle suspensions, and drops were transferred onto 5-mm wells of depression well slides (no. 101005; Carlson Scientific). The slides then were placed into 150-mm petri plates humidified with a filter paper wetted with 2.5 ml water. Dishes were sealed tightly with parafilm strips before overnight incubations at 30°C. For EM analysis, arrays were transferred onto ultrathin, formvar-removed carbon grids (no. 1882-F; Ted Pella) by placing grids on top of the drops for 1 min. Samples then were processed by placing grids on top of 100-μl water drops for 30 s, wicking from the side, staining for 45 s on 50 μl 1.3% uranyl acetate (freshly diluted and filtered), followed by blotting and air drying. For AFM analysis, drops were deposited on freshly cleaved 3 mm × 3 mm highly oriented pyrolytic graphite or mica sheets. After 1 min, the samples were rinsed with water (three times 50 μl) and then maintained under a viewing buffer (20 mM TrisHCl, pH 8.0, 100 mM KCl).

Transmission electron microscopy

Electron microscopy was performed on a JEOL JEM1200EX operated at 100 kV (Portland VA Hospital). Low-dose photography was carried out at ambient temperature, using Kodak SO163 film. Searching was performed at a magnification of 5000×, and focusing and photography were at 40,000–60,000×.

Atomic force microscopy

After specimen adsorption, samples were mounted on an E-piezoscanner of an atomic force microscope equipped with a fluid cell (Nanoscope III; Digital Instruments, Santa Barbara, CA). Calibration of the scanner was carried out with mica as the substrate reference. Cantilevers with oxide-sharpened Si_4N_4 tips (purchased from Digital Instruments) were 200 μm long and had nominal spring constants of 0.06 N/m. Initial tip engagements were performed by setting the scan size to 0 nm to minimize sample deformation. Before the samples were scanned, the operating point of the servo system was set to forces below 1 nN.

Image processing

For EM images, micrographs 100315, 100316, 121215, and 121216 were digitized at 6.53 Å/pixel and converted to MRC format images r100315b, r100315c, r100316a, r100316c, r100316d, r100316e, r121215, and r121216 (Unwin and Henderson, 1975; Baldwin et al., 1988, Henderson et al., 1990). With the use of the ICE image analysis package (Schmid et al., 1993), real space images were Fourier transformed, and diffraction patterns were indexed by hand. Lattices were refined and unbent using the MRC-derived programs MMBOX and UNBEND (Baldwin et al., 1988, Henderson et al., 1990; Schmid et al., 1993). After these steps, the calculated amplitude and phase (aph) files were edited manually to remove all low signal-to-noise reflections of IQ > 5. The acceptable reflections yielded resolutions extending to ~26 Å, and the completeness of the data was ~70% (50% in the 37–25 Å resolution shell). The best space groups for amplitudes plus phases (aph) files were determinated using the ALLSPACE program, using hexagonally indexed diffraction patterns. (Note that p6 residuals were aberrantly high when orthogonally indexed reflections were used as the ALLSPACE input.) Merging of images and determination of phase residuals were performed using unbent aph files and the program ORIGTILTB (Henderson et al., 1990). For all merges, the r100316b film was used as the reference image. Reconstruction of a real image was done using the programs CREATE TNF and FFTRANS. Files in MRC-format were then converted to TIFF format.

For AFM, 300 nm × 300 nm images were acquired at a resolution of 512 pixel/line and were exported in TIFF formats. Images then were converted to SPIDER format (Frank et al., 1988) for real space averaging steps. For averaging, raw images were Gausian low-pass filtered, and 12 140.6 Å × 140.6 Å windows were picked and summed to yield a cross-correlation reference. The reference then was used to locate cross-correlation peaks using the SPIDER (Frank et al., 1988) operation CC, and 187.5 × 187.5 $Å^2$ raw image areas, representing the top 100 cross-correlation peaks, were summed to give an average image. The quality of this image was evaluated by halving the 100 image data set, averaging the half-sets, and comparing the Fourier ring correlation (FRC) values between the averages at different resolutions, using the SPIDER operation RFM (Frank et al., 1988).

Quantification of his-MoCA bound to vesicles

For isolation of MoCA-bound membranes, 200-μl mixtures containing 25 μM his-MoCA and 250 μM PC: Ni^{2+}-DHGN 10:1 vesicles in PNG buffer, pH 8.3, were incubated overnight at 30°C and ultracentrifuged for 20 min at 165,000 × *g* (rotor Beckman TLS 55; 50,000 rpm) to pellet membranes. Supernatants were carefully discarded to remove unbound his-MoCA, and membranes were resuspended in 60 μl 10 mM MOPS (pH 7.8), 50 mM NaCl (buffer A). As controls, two other incubations were performed, with the omission of either the protein or the lipid membranes. For quantification of his-MoCA bound to vesicles using the mouse anti-CA monoclonal antibody Hy187 (Hansen et al., 1993), two 10-μl aliquots of the previously prepared his-MoCA-bound membranes were withdrawn and overlayed on the upper faces of two freshly cleaved HOPG pucks (2 cm^2) for 30 min, after which the pucks were rinsed four times with buffer A (150 μl). One puck was extracted directly with 40 μl 20 mM TrisHCl (pH 7.4), 150 mM NaCl, 1 mM EDTA, 0.1% sodium dodecyl sulfate (SDS), 1% Triton X-100, 0.5% sodium deoxycholate (IPB buffer), and the other puck was incubated with anti-CA (500 μl; 0.3 g/L in phosphate-buffered saline) for 30 min at room temperature, rinsed, and extracted as decribed above. As controls, 10-μl aliquots of his-MoCA bound membranes and membranes alone were incubated in solution with the anti-CA antibody (500 μl; 0.3 g/L) for 30 min, after which the antibody/his-MoCA/membrane complexes were pelleted by a second ultracentrifugation and were suspended in IPB buffer. For protein analysis, samples were subjected to SDS-polyacrylamide gel electrophoresis (SDS-PAGE), and gels were electroblotted onto a nitrocellulose filter. Gag proteins were immunodetected with the mouse anti-CA antibody Hy187, which was revealed by using an alkaline phosphatase-conjugated anti-mouse antibody at 1:12,550 dilution, followed by a color reaction (Hansen et al., 1993). The secondary antibody plus color reaction steps also revealed nitrocellulose-bound anti-CA heavy and light chains from the incubations described above.

RESULTS

Preparation and analysis of lipid vesicles

Retrovirus particles have proved somewhat intractable to structural analysis, as they are enveloped with a cellularly derived lipid bilayer and are heterogeneous in size and

shape (Fuller et al., 1997; Yeager et al., 1998). Because of this, we designed a method for the analysis of how the major structural (Gag) proteins of the Moloney murine leukemia virus (M-MuLV) organize on membranes in immature virus particles (Barklis et al., 1997). Briefly, N-terminally his-tagged Gag protein derivatives assembled on monolayers containing the nickel-chelating lipid DHGN can be lifted onto electron microscope grids and analyzed by transmission EM (see Fig. 1). This model system is faithful in that in vitro assembly occurs on a membrane, with the his-tag/DHGN interaction substituting for the membrane-anchoring function of a myristate group, which modifies the M-MuLV Gag protein amino-terminus in vivo (Rein et al., 1986).

To complement EM analyses, we decided to adapt our system for analysis of membrane-bound Gag proteins under buffer solution by AFM. Initially, we attempted to transfer monolayers onto octadecyl-silanized mica and glass substrates. Silanization was by octadecyltrichlorosilane treatment of cleaned glass or freshly cleaved mica surfaces (Egger et al., 1990). However, silanization of mica appeared incomplete, and hydrophobic glass substrates were suboptimal for AFM as a consequence of poor monolayer transfer and rapid loss of image quality during AFM scanning with silicon nitride (Si_4N_4) tips (data not shown).

As an alternative to monolayer lifts, and to mimic cellular plasma membranes, we next opted to prepare Ni^{2+}-DHGN-containing lipid bilayers as Gag protein assembly targets. Unilamellar vesicles were prepared by sonication of dried lipids to final lipid concentrations of 500 μM PC and 50 μM Ni^{2+}-DHGN (see Materials and Methods). Vesicles so prepared were processed by 4 h of adsorption on freshly cleaved mica, followed by two gentle rinses with water and then viewing buffer. Samples then were imaged under viewing buffer with an oxide-sharpened Si_4N_4 tip at 2.0 Hz in contact mode (Fig. 2). After 4 h of adsorption to mica, vesicles appeared to be intact but heterogeneous in size, with diameters from 100 nm to 500 nm (Fig. 2 *a*). Heights ranged from 7.3 to 7.6 nm, with an occasional measurement of approximately twice that height (Fig. 2 *b, left side*). In this regard, because of strong elasticities observed for these samples, it is noteworthy that imaging was only possible by application of 5–10-nN forces. Given these high scan forces and assuming a bilayer thickness of 4–5 nm (Simon and McIntosh, 1984; Sackmann, 1983), our average apparent height of 7.5 nm is consistent with those of flattened, unilamellar vesicles, while higher features may result from the stacking of two vesicles. While 4-h preparations appeared as flattened but elastic vesicles, after aging of substrate-bound vesicle preparations overnight, AFM imaging could be achieved with scan forces below 1 nN and lipids spread over areas of 200-1000 μm in diameter (Fig. 2 *c*). The heights of such areas were relatively constant at 3.1 $\pm$ 0.2 nm (Fig. 2 *d*), within the expected range of lipid bilayers in a fluid state and imaged by AFM (Mou et al., 1995). These observations suggest that initially substrate-bound vesicles converted to single bilayers after overnight incubations and are consistent with previous observations (Mou et al., 1994).

EM imaging of bilayer-bound M-MuLV capsid protein two-dimensional arrays

As noted above, while lipid bilayers could be imaged conveniently by AFM (Fig. 2), monolayer imaging gave poor results. Consequently, any AFM images of membrane-bound proteins we hoped to obtain would have to be compared with EM images of lipid bilayer-bound proteins,

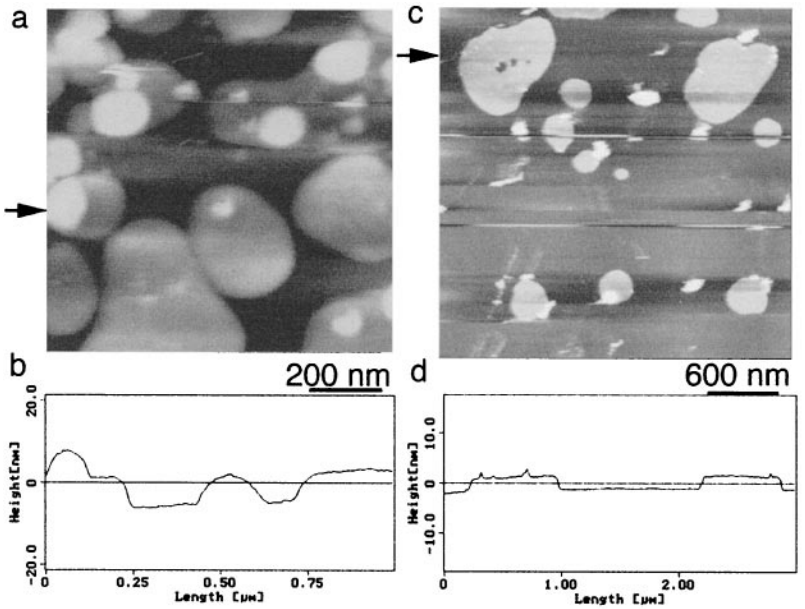

FIGURE 2 AFM imaging of PC+Ni^{2+}-DHGN vesicles and bilayers. Shown are AFM images of vesicles containing Ni^{2+}-DHGN and phosphatidylcholine after 4 h (*a*) and overnight (*c*) adsorption to freshly cleaved mica. *b* and *d* show cross-sectional heights of images *a* and *c*, respectively, at the levels marked by the arrows. Initial mica-bound vesicles (*a*) with apparent heights ranging from 7.3 to 7.6 nm (*b*) were converted overnight to single bilayers (*c*) with thicknesses of 3.1 $\pm$ 0.2 nm (average of 14 mesurements from different sections). Scanning was performed in contact mode using a fluid cell, employing 200-μm-long oxide-sharpened Si_4N_4 tips, with nominal spring constants of 0.06 N/m. Imaging was done under a viewing buffer (20 mM TrisHCl pH 8.0, 100 mM KCl), with applied forces of ~5–10 nN (*a, b*) and 1 nN (*c, d*) and scan frequencies of 2.0 Hz. Frame sizes were 1 μm for *a* and 3 μm for *c*, and resolutions were 512 pixels/line. The full gray-level ranges of *a* and *b* were 30 and 25 nm, respectively.

rather than the monolayer-associated protein images obtained previously (Barklis et al., 1997). Because of this, we undertook the EM analysis of his-tagged M-MuLV capsid (his-MoCA) proteins bound to lipid bilayers. To do so, optimization experiments were undertaken. In agreement with previous data (Barklis et al., 1997), optimal conditions involved incubation in 50 mM sodium phosphate (pH 8.3), 5 mM sodium acetate, 10 mM imidazole, 250 mM NaCl, 20% glycerol (PNG buffer), using a PC:Ni-DHGN ratio of 10:1. We also observed that array formation was optimal at a lipid-to-protein concentration ratio of 10:1 (250 μM lipid:25 μM his-MoCA), slightly lower than the ratio predicted assuming a lipid surface area of 70 Å^2/molecule (Schmitt et al., 1994; Mingotaud et al., 1993) versus 910 Å^2/molecule for a his-MoCA monomer (Barklis et al., 1997).

Using the above conditions in overnight, 30°C incubations, crystalline his-MoCA arrays made on vesicles were apparent by EM of negatively stained samples. As shown in Fig. 3 *a*, vesicle incubations in the presence of his-MoCA resulted in the appearance of large membranes with extensive his-MoCA crystalline arrays, which were more obvious at higher magnification (Fig. 3 *b*). A number of calculated diffraction patterns from such arrays were twinned, possibly resulting from arrays formed on opposite sides of a vesicle or from separate but adjacent crystals. However, frequently untwinned patterns were observed, as in Fig. 3 *c*. The diffraction patterns (Fig. 3 *c*) could be indexed in either a

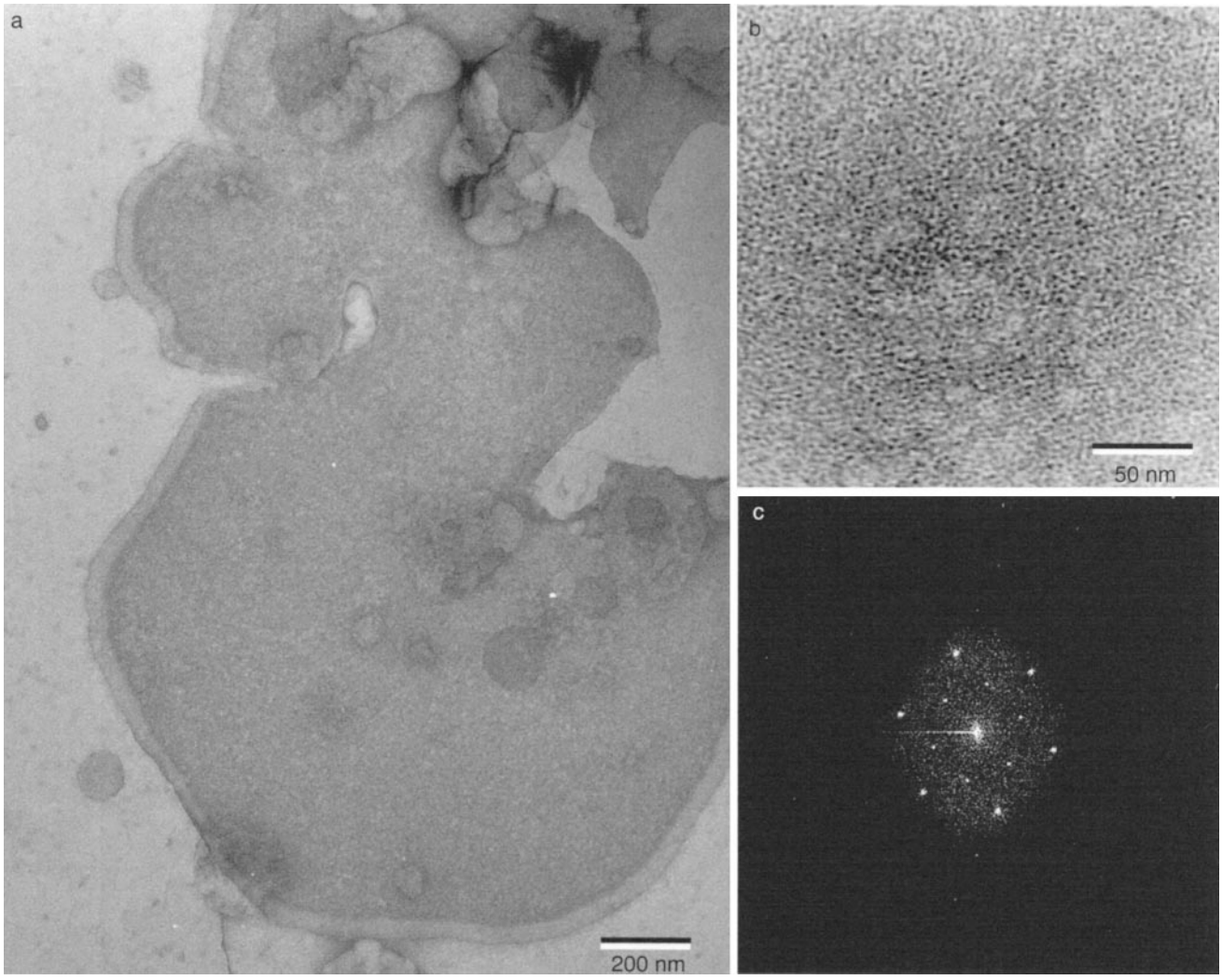

FIGURE 3 EM of liposome-bound his-MoCA proteins. His-MoCA proteins and suspensions of PC/Ni^{2+}-DHGN vesicles in PNG buffer, pH 8.3, were incubated overnight at 30°C, transfered to ultrathin carbon grids, washed, and uranyl acetate stained. (*a*) Electron micrograph showing his-MoCA bound membrane. The size bar represents 200 nm. (*b*) High-magnification image of his-MoCA proteins arrayed on a lipid bilayer. The scale bar represents 50 nm. (*c*) Shown is the calculated diffraction pattern for the stained his-MoCA 2D image. The pattern can be indexed in a hexagonal or orthorhombic fashion. The innermost six reflections and higher resolution reflections are barely visible in this contrast range, while the six brightest reflections at 0.0254 Å^{-1} correspond to the 1,1; -1,2; -2,1; -1,-1; 1,–2; and 2,–1 reflections for a gamma = 60° unit cell or 2,0; 1,3; -1,3, -2,0; -1,-3; and 1,–3 reflections for a gamma = 90° unit cell.

hexagonal ($a^* = b^* = 0.0142$ Å^{-1}, $\gamma^* = 60°$) or orthogonal ($a^* = 0.0123$ Å^{-1}, $b^* = 0.0074$ Å^{-1}, $\gamma^* = 90°$) fashion, with reflections (not visible in Fig. 3 *c*) out to 25.4 Å (orthogonal reflection 1, 5), similar to what we have obtained with negatively stained monolayer arrays. Averaging of eight untwinned diffraction patterns indexed in an orthogonal fashion yielded a mean unit cell of $a = 81.5 \pm 0.3$ Å, $b = 135.3 \pm 1.8$ Å, and $\gamma = 89.1 \pm 1.4°$, while the corresponding hexagonal unit cells were $a = 81.2 \pm 0.5$ Å, b = 79.6 ± 1.7 Å, $\gamma = 117.9 \pm 1.5°$ (see Table 1). As shown in Table 1, his-MoCA proteins formed arrays that were consistent with hexagonal (p6) space group symmetry, giving an average phase residual of 18.1 ± 4.5° to 15-Å resolution. Phase residual values for trigonal (p3) symmetry calculations were slightly better than those for the p6 space group (13.5 ± 5.2 at 15-Å resolution; Table 1), suggesting that it may be a more appropriate space group designation for his-MoCA crystals; implications with regard to protein packing will be discussed below (see Discussion).

Comparison of calculated diffraction patterns of bilayer-bound his-MoCA, assuming no symmetry constraints (p1), showed good agreement between images, with phase residuals less than 30° at 26 Å or lower (Table 1). Back-transformation of unbent, filtered diffraction patterns resulted in 2D projection reconstructions, as shown in Fig. 4, *A–C*. As illustrated, the M-MuLV capsid protein assembled into cage-like structures on PC/Ni^{2+}-DHGN bilayers. On inspection, there appeared to be distinct types of protein-free cage holes (*dark*), which were surrounded by six electron-dense (*white*) units, apparently representing protein monomers. Reconstructions showed two or three types of cage holes (*numbered in A–C*). In all panels, the no. 1 cage holes appeared distinct, as observed previously (Barklis et al., 1997). However, it was unclear whether the no. 2 and no. 3 holes were distinct, as predicted by p3 symmetry, or similar, consistent with p6 symmetry (see Discussion). In any case, each cage hole was spaced 45.5 Å from its nearest-neighbor cage holes, and spacings between putative distinct cage hole types (Fig. 4, *A–C, 1 to 1, 2 to 2*, and *3 to 3*) were 81.5 Å. These distances are consistent with those observed for M-MuLV capsid proteins assembled on lipid monolayers (Barklis et al., 1997), as well as the apparent spacing of PrGag proteins in immature M-MuLV particles (Yeager et al., 1998).

AFM imaging of his-MoCA bound to lipid bilayers

Based on our imaging of lipid membranes by AFM (Fig. 2), we opted to image his-MoCA proteins on lipid bilayers. To do so, his-MoCA proteins were incubated overnight at 30°C with PC/Ni^{2+}-DHGN vesicles, deposited on mica or highly oriented pyrolytic graphite (HOPG), and imaged under 20 mM TrisHCl, 200 mM KCl (pH 8.0). Scanning was performed in contact mode with a Nanoscope III fluid cell, operated without the O-ring, employing 200-μm-long oxide-sharpened Si_4N_4 tips, with nominal spring constants of 0.06 N/m. After tip engagement, to locate membrane areas, slow scans (2 Hz) were performed on 1–25 μm^2 areas. As illustrated (Fig. 5 *a*), bilayer areas as large as several hundred nanometers to microns were observed. In contrast to bilayers composed only of lipid (Fig. 2 *c*), areas of his-MoCA- bound bilayers (Fig. 5 *a*) revealed features as tall as 8.5–10.6 nm, consistent with membrane heights of 3.0–4.0 nm plus M-MuLV capsid protein heights of ~6 nm. Slight differences between height measurements made on different dates may be related to the utilization of different tips, which yielded different compression forces on the membrane. At higher topologies, his-MoCA-bound membranes (Fig. 5 *c*) showed patches of arrays, comprising apparent 0.33 ± 0.06 nm depressions spaced at ~8.0-nm intervals, and calculated diffraction patterns (Fig. 5 *d*) demonstrated an apparent sixfold symmetry (two reflections are obscured by the *y* axis), corresponding to a unit cell of $a = b = 7.9$ nm, $\gamma = 60°$.

The his-MoCA arrays as imaged by AFM (Fig. 5) did not yield crystals that were compatible with conventional 2D diffraction analysis. However, it was possible to perform real space averaging operations using the SPIDER suite of image reconstruction programs (Frank et al., 1988). To do so, 12 140.6 × 140.6 Å^2 windows were added from low-pass filtered images to yield a cross-correlation reference image, which was used to identify the top 100 cross-correlation peaks from his-MoCA AFM scans. After this step, the

TABLE 1 Comparison of EM images

File name	Orthorhombic cell			Space group fit phase residual (°)				Interimage phase residual (°)
	a (Å)	*b* (Å)	γ (°)	p1	p2	p3	p6	
r100316cU	81.7	135.4	90.0	25.5	31.4	11.2	18.3	—
r100316aU	82.1	133.1	89.7	26.0	22.0	9.4	14.2	15.5
r100316dU	81.1	133.1	89.7	23.8	28.3	9.9	17.3	17.0
r100316eU	81.5	136.2	87.0	31.8	22.7	12.1	16.7	28.1
r121215U	81.1	133.7	90.4	26.9	32.9	21.1	24.3	26.1
r121216U	81.6	136.1	90.8	28.9	23.9	6.9	10.8	24.7
r100315bU	81.3	137.6	88.4	31.4	36.8	18.4	23.6	10.1
r100315cU	81.5	137.3	87.6	31.9	32.7	19.0	19.8	14.3

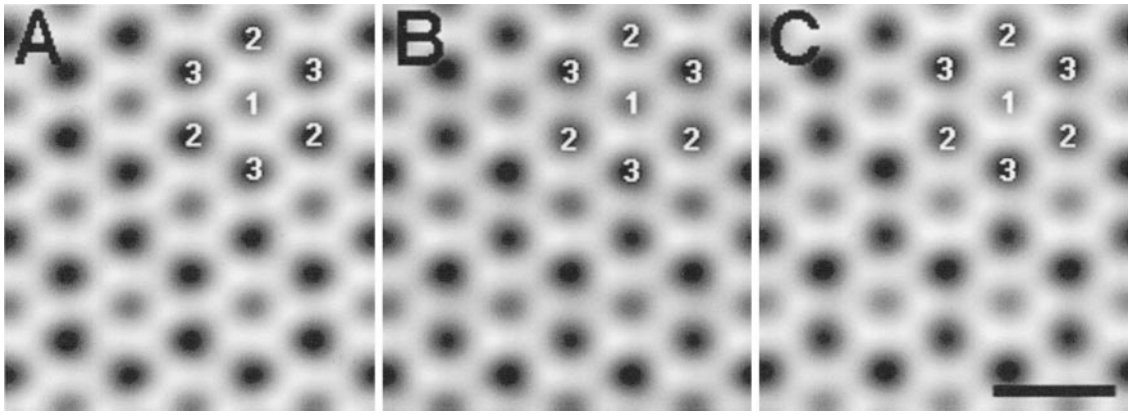

FIGURE 4 EM projection structure of vesicle-bound his-MoCA. Shown are 2D projection reconstructions of his-MoCA proteins bound to PC/Ni^{2+}-DHGN vesicles. The scanned images r121216c (*A*), r121216 (*B*), and r121215 (*C*) were Fourier transformed, unbent, filtered, and back-transformed with no symmetry constraints to yield the 2D projections. Note that in all panels of the figure, protein regions are in white, and the protein-free areas appear dark, while putative different cage hole types are numbered. The size bar in *C* corresponds to a distance of 80 Å in all three panels.

corresponding 187.5 × 187.5 $Å^2$ image areas from unfiltered scans were added to give an averaged AFM image of membrane-bound his-MoCA proteins. As illustrated (Fig. 6), the topology of the bilayer-bound proteins shows a lattice of higher features surrounding shallow depressions spaced at 7.9-nm distances, reminiscent of hole-to-hole spacing between similar cage holes from EM micrographs (Fig. 4). The quality of our AFM reconstruction was assessed by halving our data set, generating two independent reconstructions, and comparing the averaged images with each other by determination of Fourier ring correlation (FRC) values. By this method, we found FRC values dropped from 0.93 (highly correlated) to 0.53 at 0.032 $Å^{-1}$, yielding a practical resolution limit of ~31 Å.

Quantification of MoCA bound to membrane.

Although the above AFM results clearly showed the existence of a cage-like lattice, it was unclear whether the lattice corresponded to the protein or lipid sides of his-MoCA bound membranes. To disciminate between these possibilities, we tested whether his-MoCA proteins (Fig. 7, *lane 1*) on substrate-bound membranes were accessible to binding by the anti-MoCA monoclonal antibody Hy187 (Fig. 7, *lane 2*; Hansen et al., 1993). For these experiments, we prepared PC/Ni^{2+}-DHGN vesicles and PC/Ni^{2+}-DHGN vesicles with bound his-MoCA proteins (his-MoCA vesicles). Not surprisingly, while 35-kDa his-MoCA proteins in his-MoCA vesicles were pelleted by centrifugation (Fig. 7, *lane 3*), free his-MoCA proteins were pelleted much less efficiently (Fig. 7, *lane 6*). Also, as expected, the 50-kDa and 25-kDa heavy and light chains of the anti-MoCA antibody bound well to his-MoCA containing vesicles (*lane 4*) but not nearly as well to the naked PC/Ni^{2+}-DHGN vesicles (*lane 5*). Analysis of the orientation of his-MoCA proteins on substrate-bound bilayers involved binding reactions on HOPG, which served as a substrate for our AFM studies on his-MoCA arrays (Fig. 5). Our procedure involved binding proteins or vesicles to HOPG, postbinding steps with anti-MoCA, and detection of his-MoCA and anti-MoCA proteins by electrophoresis and immunoblotting after release from the HOPG substrate. As indicated in Fig. 7, the free his-MoCA protein has some capacity for binding to HOPG by itself (*lane 10*), while his-MoCA vesicles appeared to bind quite efficiently to HOPG (*lane 9*). Significantly, anti-MoCA, which bound well to his-MoCA vesicles in solution (*lane 4*), bound poorly to substrate-bound his-MoCA vesicles (*lane 9*). Indeed, while the amount of substrate-bound anti-MoCA in lane 9 exceeded the level of direct anti-MoCA binding to HOPG (*lane 11*), it was approximately equal to the amount that adhered to HOPG-bound PC/Ni^{2+}-DHGN vesicles (*lane 12*). Furthermore, on a proportional basis, the amount of anti-moCA bound to HOPG via his-MoCA vesicles (*lane 9*) appeared to be much reduced relative to the level of anti-MoCA bound via free his-MoCA to HOPG (*lane 13*). These results indicate that membrane-bound his-MoCA proteins on AFM supports were not readily accessible to antibody binding and thus imply that these retroviral Gag proteins were sandwiched between PC/Ni^{2+} DHGN membranes and HOPG substrates during AFM imaging.

DISCUSSION

Moloney murine leukemia virus, like its C-type retrovirus conterparts, assembles at the plasma membranes of infected cells, and the expression of the M-MuLV Gag polyprotein is sufficient for the assembly of immature virus particles. Normally, during or after budding, cleavage of the Gag proteins by the viral protease results in a morphological change from an immature to a mature virus form (Coffin et al., 1997). Recent cryo-EM studies of immature retrovirus

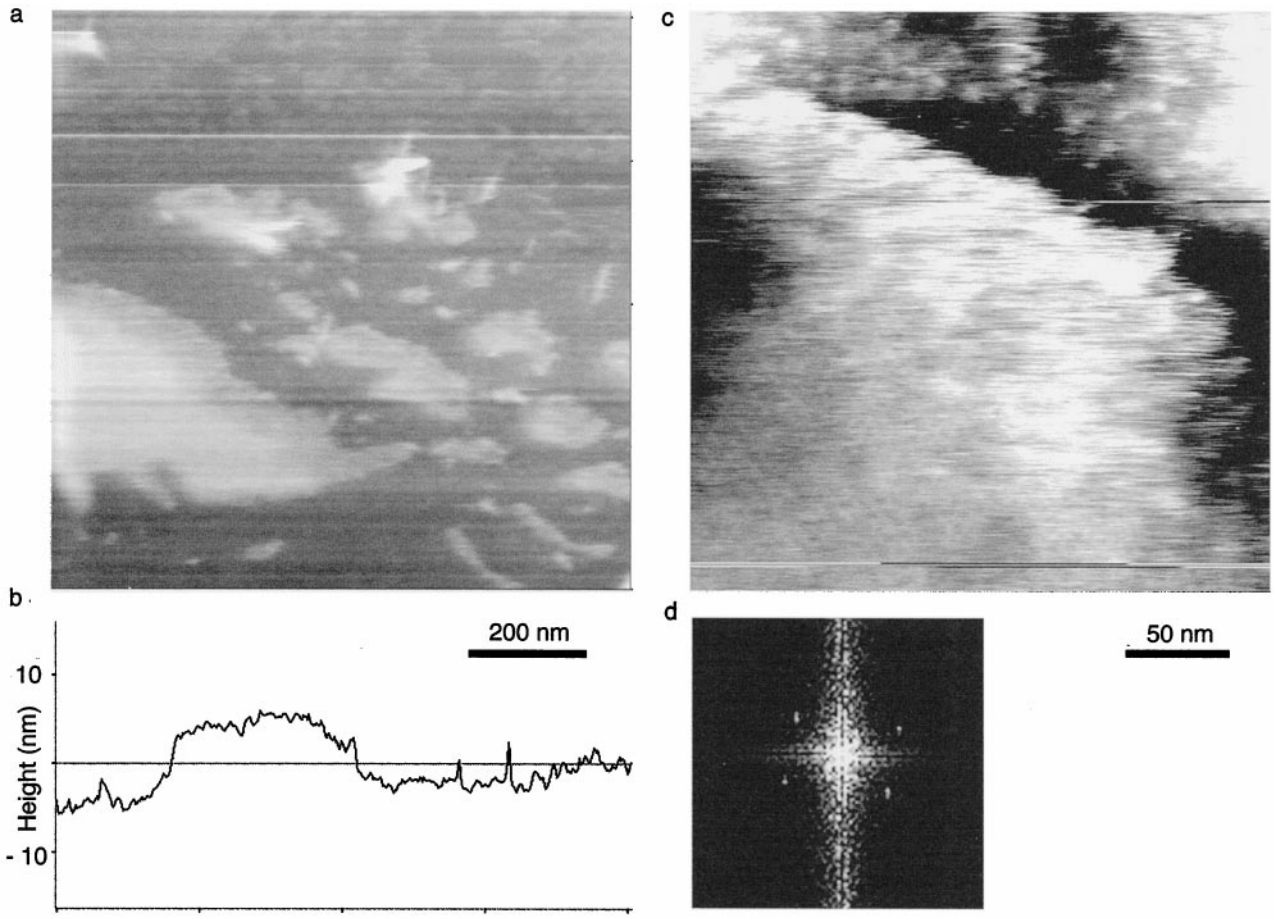

FIGURE 5 AFM imaging of bilayer-bound his-MoCA protein arrays. Samples of his-MoCA bound to PC plus Ni^{2+}-DHGN bilayers were adsorbed onto AFM substrates as described in Materials and Methods. Scanning was performed at ambient temperature (21–23°C) in contact mode, using a Nanoscope III fluid cell and employing 200-μm-long oxide-sharpened Si_4N_4 tips, with nominal spring constants of 0.06 N/m. Imaging was done under a buffer (20 mM TrisHCl, pH 8.0; 100 mM KCl) with applied forces of ~0.5 nN and scan frequencies of 2.0 Hz. (*a*) A low-resolution AFM scan showing variously sized his-MoCA/PC plus Ni^{2+}-DHGN membrane patches. The size bar indicates 200 nm. (*b*) A cross-sectional height plot taken from the lower left to upper left section of *a*. The abscissa marks indicate 200 nm, and the ±10 nm height marks are shown on the ordinate axis. The full gray-level range of the scan is 20 nm, and the apparent membrane height in this scan is 8.5 nm, although scan heights were observed to vary from 8.5 to 10.6 nm. (*c*) A high-resolution, small scan size image of his-MoCA/PC plus Ni^{2+}-DHGN, taken at a full gray-level height range of 2 nm is shown. The cage-like array of protein with 0.33 ± 0.06 nm depressions spaced at ~8.0-nm intervals is visible at the lower left. The size bar indicates 50 nm. (*d*) The power spectrum from the lower left-hand third of *c*, calculated using the Nanoscope III power spectrum option, appears hexagonal, although two reflections are obscured by the *y* axis. The reflections correspond to a real space distance of 7.9 nm.

particles have shown that Gag polyproteins associate to form paracrystalline sheets, but the subsequently formed spherical virus shells apparently lack icosahedral symmetry (Fuller et al., 1997; Yeager et al., 1998). Unfortunately, natural retrovirus particle pleomorphism and difficulties in preparation of homogeneous virus preparations have hampered the analysis of immature and mature retrovirus particles (Nermut et al., 1994; Fuller et al., 1997; Yeager et al., 1998). To circumvent the above difficulties, we designed a model system for the study of the assembly of Gag proteins on the face of a lipid membrane (Barklis et al., 1997, 1998). The approach employs a his-tagged retrovirus capsid domain and membranes consisting of PC and a nickel-chelating lipid, DHGN. Here, we have focused on the M-MuLV capsid domain because it mediates critical Gag-Gag contacts, and it is not sensitive to proteolysis.

As observed in monolayer experiments (Barklis et al., 1997), his-tagged Gag proteins formed regular arrays on PC/Ni^{2+}-DHGN vesicles (Fig. 3). Diffraction analysis indicated that vesicle-bound his-MoCA proteins formed consistent, 2D crystals (Table 1). Two-dimensional projection reconstruction shows that the proteins formed cages composed of cage holes spaced at 45–46-Å intervals (Fig. 4), in agreement with studies on immature M-MuLV particles (Yeager et al., 1998). The appearance of reconstructions suggests that the no.1 holes in Fig. 4, *A–C*, are hexagonally symmetrical, consistent with a p6 space group assignment. However, if slight differences in no. 2 and no. 3 holes are

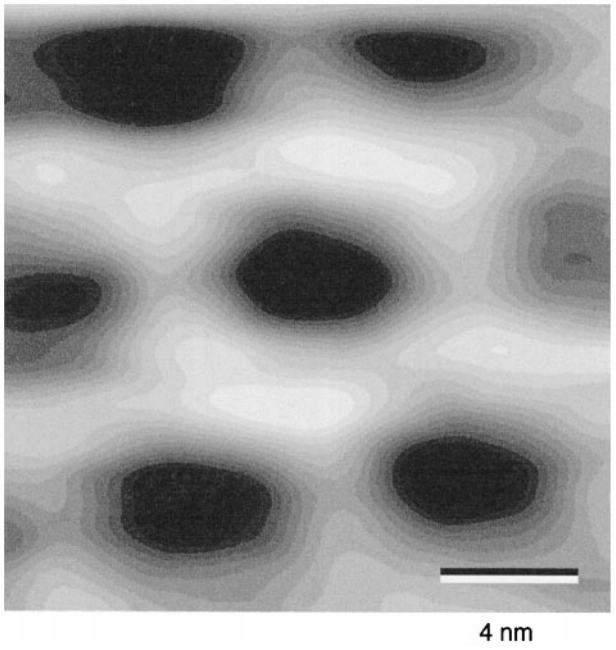

FIGURE 6 Averaged AFM image of his-MoCA proteins bound to lipid bilayers. Twelve 140.6 × 140.6 Å^2 low-pass-filtered AFM windows of membrane-bound his-MoCA arrays were added using the SPIDER real space AD operation to yield a cross-correlation reference image, which was employed in the CC operation to identify the top 100 cross-correlation peaks from a 300 × 300 nm^2 his-MoCA AFM scan. Cross-correlation peak locations were used to cut the corresponding 100 187.5 × 187.5 Å^2 unfiltered image windows using the SPIDER WI operation, and the windows were added (SPIDER operation AS R) to yield the averaged 187.5 × 187.5 Å^2 AFM image, where higher features are white and lower features are dark. Note that spacing between depressions is ~8.0 nm and that the size bar corresponds to 4 nm. The quality of the reconstruction was assessed by halving the 100-image data set and comparing the two half-averages by Fourier ring correlation (FRC), using the SPIDER operation RF M. By the use of this method, the 50 image averages showed FRC values of 0.93 (highly correlated) at 0.011 Å^{-1}, dropping to 0.53 at 0.032 Å^{-1}, giving an effective resolution limit of ~31 Å.

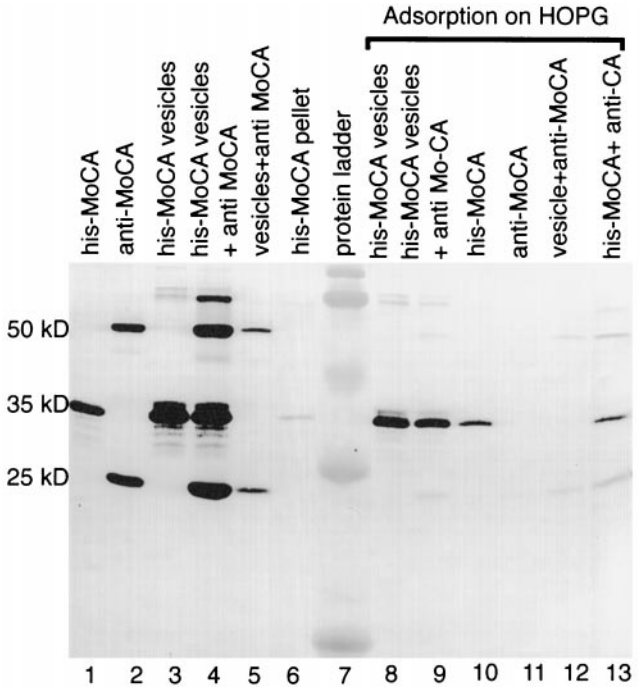

FIGURE 7 Orientation of membrane-bound his-MoCA proteins on AFM substrates. The 35-kDa his-MoCA and Hy187 anti-MoCA heavy chain (50 kDa) and light chain (25 kDa) proteins bound in incubations to membranes and substrates were detected after the extraction of proteins, gel electrophoresis, electroblotting onto nitrocellulose, and immunodetection as described in Materials and Methods. Incubations included only proteins (*lanes 1, 2, 6*), proteins plus PC/Ni^{2+}-DHGN vesicles (*lanes 3–5*), or protein and membrane combinations on HOPG AFM substrates. Lane designations indicate samples as follows: *1*, 4 μg (120 pmol) his-MoCA; *2*, 12 μg (80 pmol) anti-MoCA; *3*, his-MoCA vesicles, purified by centrifugation after a 0.2-ml, 250 μM PC/Ni^{2+}-DHGN, 25 μM his-MoCA incubation; *4*, his-MoCA vesicles, postincubated with 1 nmol anti-MoCA and repurified; *5*, PC/Ni^{2+}-DHGN vesicles (containing no his-MoCA), postincubated with 1 nmol anti-MoCA and repurified; *6*, 29 μg (0.83 nmol) his-MoCA, processed to simulate vesicle purification conditions; *7*, protein size standard; *8*, his-MoCA vesicles bound to HOPG; *9*, HOPG-bound his-MoCA vesicles (if 100% recovery in pellet: 0.83 nmol his-MoCA; 8.3 nmol PC/Ni^{2+}-DHGN) postincubated with 1 nmol anti-MoCA and washed; *10*, 29 μg (0.83 nmol) his-MoCA bound directly to HOPG and washed; *11*, 150 μg (1 nmol) anti-MoCA bound directly to HOPG and washed; *12*, HOPG-bound PC/Ni^{2+}-DHGN vesicles (containing no his-MoCA; 8.3 nmol PC/Ni^{2+}-DHGN if 100% pellet recovery) postincubated with 1 nmol anti-MoCA and washed; *13*, 29 μg (0.83 nmol) his-MoCA bound directly to HOPG, washed, then postincubated with 1 nmol anti-MoCA and washed. The molecular masses of the proteins in the standard lane are 97, 68, 43, 29, and 18 kDa.

verified in future, higher resolution studies, the lower symmetry p3 assignment may prove more appropriate.

Assuming a p6 packing arrangement, Fig. 8 *A* shows a model for M-MuLV capsid protein assembly at a membrane. This model shows hexagonal and trigonal cage holes, each surrounded by six CA monomers. Features of the model are that it accounts for p6 symmetry, and head-to-head CA homodimers (Gamble et al., 1997; shown as hexagon pairs joined by no. 4–no. 4 interfaces) and CA surfaces (idealized as numbers on hexagons) occupy constant positions within the network. An alternative model, which allows for three different types of cage holes, is shown in Fig. 8 *B*. The model is compatible with p3 symmetry, but does not directly account for the existence of head-to-head dimers (Gamble et al., 1997); requires that CA subdomains must fulfill two different roles (as where hexagon no. 1 and no. 2 faces both form dimer interfaces and cage hole edges); and presents an ambiguous assembly pathway.

In comparison with EM results, AFM analyses gave similar yet slightly different results (Figs. 5 and 6). For AFM studies, we found that his-MoCA-bound PC/Ni^{2+}-DHGN vesicles adhered to subtrates to yield image heights of 8.5–10.6 nm (Fig. 5), consistent with a lipid bilayer height of 3.0–4.0 nm, plus a his-MoCA layer height of ~6 nm. As demonstrated in Fig. 7, the his-MoCA layer appeared inaccessible to antibody probing, supporting the notion that his-MoCA proteins were sandwiched between

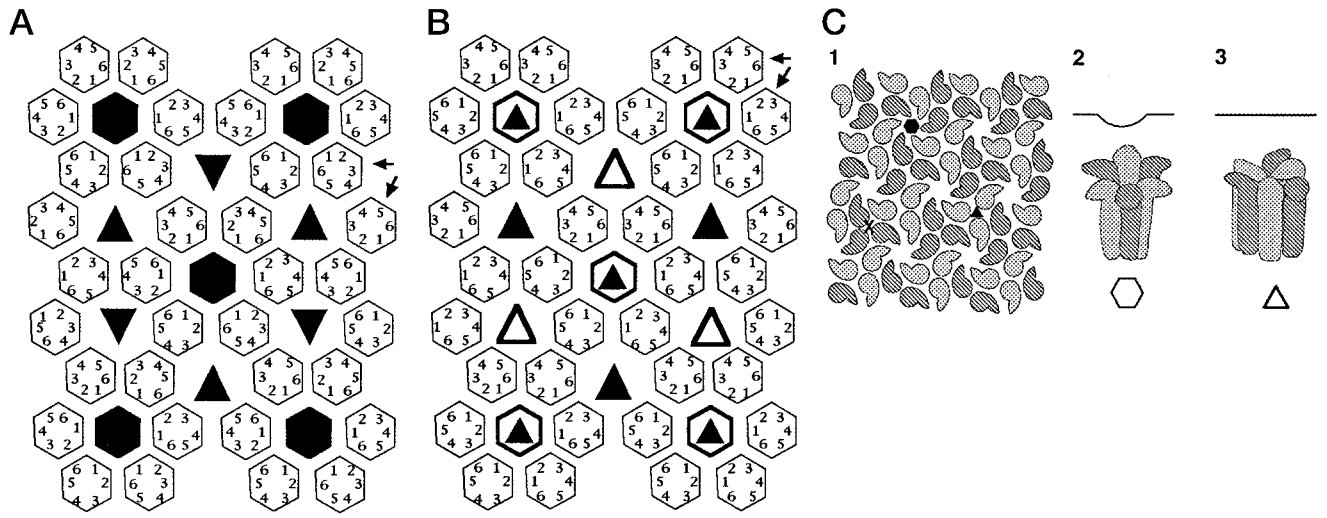

FIGURE 8 Models of murine retrovirus capsid assembly on a lipid bilayer. (*A*) A model of M-MuLV CA proteins organized on a membrane and showing p6 symmetry. Protein monomers are depicted as hexagons with numbered faces, and protein-free cage holes are either hexagonally (*black hexagons*) or trigonally (*black triangles*) symmetrical. The model predicts head-to-head dimer building blocks (*arrows at the upper right*) and unique environments for each monomer face. It is compatible with a p6 space group assignment. (*B*) The trigonal (p3) model of his-MoCA assembly on membranes features monomers (face-numbered hexagons) surrounding three different types of cage holes (*black triangles, white triangles, and triangles in hexagons*, which signify cage holes that appear most hexagonal). Assembly is postulated to occur from asymmetrical head-to-head dimer building blocks (*arrows at the upper right*), where dimer formation is initiated at vertices between the no. 1 and no. 2 faces. An assembly constraint is that adjacent no. 3 and no. 6 sides on dimer units are unavailable for interprotein contacts, while separated no. 3 and no. 6 sides mediate formation of hexamer building blocks. (*C*) In this model to correlate EM and AFM results, capsid monomers are depicted as commas (*picture 1*) or as deformed rods in three dimensions (*pictures 2, 3*). Note that the membrane-proximal CA domains are oriented up in pictures 2 and 3 and are depicted as the globular portions of commas in picture 1. (*1*) Schematic model of his-MoCA assemblies viewed from the bilayer side. Two different cage holes, corresponding to the triangle and hexagon holes from *A*, are indicated, although the model is consistent with the scheme in *B*, assuming that cage holes similar to the one marked by the X are a distinct type. (*2*) An arrangement of his-MoCA monomers surrounding a cage hole that can be detected by AFM. In this depiction, the cage hole represents the hexagon holes from *A*, with membrane-proximal protein regions oriented upward. As illustrated above the protein units, AFM scanning of arrays is expected to identify shallow depressions. (*3*) The predicted arrangement of his-MoCA proteins surrounding a second type of cage hole, with protein units oriented as in picture 2. These cage hole locations are not expected to be observed by AFM. Note that for a trigonal model, a third type of cage hole (marked by the X in *A*) would appear similar to the cage holes shown here, except that darkly and lightly shaded monomer units would be switched.

bilayers and substrates during AFM imaging. Our observations suggest that his-MoCA-decorated vesicles adhered to supports by protein-substrate binding, followed by vesicle breakage, and inside-up bilayer unrolling, a hypothesis that is consistent with previous results (Mou et al., 1994) and our own observations with PC/Ni^{+2}-DHGN vesicles (Fig. 2). Although his-MoCA proteins appeared to be covered by bilayers during AFM analyses, by using moderate (0.5 nN) force with low spring constant (0.06 N/m) cantilevers it was possible to image membrane-bound arrays under buffer (Fig. 5). Under these conditions, proteins would not be expected to be imaged directly. Rather, bilayer regions supported by proteins would appear as higher features, while membrane regions that covered protein-free regions of his-MoCA cages could be deformed by tip forces, appearing as depressions. In contrast to EM results (Fig. 4), we found that the membrane surfaces of his-MoCA arrays showed evidence of only one type of cage hole. Specifically, shallow depressions of 0.33 ± 0.06 nm were observed to be spaced at 7.9-nm hole-to-hole distances (Figs. 5 and 6).

Because AFM images show surface topologies and EM images represent 2D projections of electron densities, there are numerous ways in which AFM and EM results can be reconciled. However, other observations reduce the number of possible models. Notably, CA proteins are composed of two domains (Fuller et al., 1997; Yeager et al., 1998; Gitti et al., 1996), and cage holes appear to be formed by hexamer rings (Barklis et al., 1997, Fig. 4). Given these results and making the assumption that AFM cage hole positions correspond to one type of EM cage hole, models must explain how one type of cage hole appears to be more electron dense than the others, while two-thirds of the cage holes are supported well enough to resist deformation by AFM tips. One model that satisfies the above restrictions is depicted in Fig. 8 *C*. As shown, each CA monomer is modeled as a hockey stick or golf club, with the club ends adjacent to lipid monolayers. Club heads point away from one type of cage hole (Fig. 8 *C, 1, 2*) and toward the other holes (an example is shown in Fig. 8 *C3*). While the model obviously remains hypothetical, several of its implications are pertinent for consideration. In particular, the two domains of CA monomers interact most closely with different partners in membrane-bound arrays. Moreover, while membrane-bound his-MoCA EM projections show cages with

two or three hexamer types (Figs. 4 and 8), our model, with slight adjustment, is consistent with the hexamer-trimer cages that HIV capsid proteins form on monolayers (Barklis et al., 1998). Furthermore, the arrangement shown implies that the cytoplasmic tails of M-MuLV envelope protein trimers, which penetrate immature M-MuLV cores, would do so via one type of cage hole, suggesting a maximum of one Env protein trimer per six Pr^{Gag} monomers. We are currently testing these predictions and implications in vivo and in vitro.

We thank Jason McDermott, Sonya Karanjia, and Doug Huseby for helpful discussions, and we are indebted to one of our manuscript reviewers, whose patient advice improved the accuracy and interpretation of our data.

This research was supported by a grant from the National Institutes of Health (5R01 GM 52914) to EB and fellowship support to GZ from the Association pour la Recherche sur le Cancer (ARC) and the Human Frontier Science Program Organization.

REFERENCES

Baldwin, J., R. Henderson, E. Beckman, and F. Zemlin. 1988. Images of purple membrane at 2.8 Å resolution obtained by cryo-electron microscopy. *J. Mol. Biol.* 202:585–591.

Barklis, E., J. McDermott, S. Wilkens, S. Fuller, and D. Thompson. 1998. Organization of HIV-1 capsid proteins on a lipid monolayer. *J. Mol. Chem.* 273:7177–7180.

Barklis, E., J. McDermott, S. Wilkens, E. Schabtach, M. F. Schmid, S. Fuller, S. Karanjia, Z. Love, R. Jones, Y. Rui, X. Zhao, and D. Thompson. 1997. Structural analysis of membrane-bound retrovirus capsid proteins. *EMBO J.* 16:1199–1213.

Binnig, G., C. F. Quate, and C. Gerber. 1986. Atomic force microscopy. *Phys. Rev. Lett.* 56:930–933.

Brown, H., J. Troncoso, and J. Hoh. 1998. Neurofilament-L homopolymers are less mechanically stable than native neurofilaments. *J. Microsc.* 191:229–237.

Campbell, S., and V. Vogt. 1995. Self-assembly in vitro of purified CA-NC proteins from Rous sarcoma virus and human immunodeficiency virus type 1. *J. Virol.* 69:6487–6497.

Coffin, J. M., S. H. Hughes, and H. E. Varmus. 1997. Retrovirus. Cold Spring Harbor Laboratory, Cold Spring Harbor, NY.

Czajkowsky, D., S. Sheng, and Z. Shao. 1998. Staphylococcal alpha-hemolysin can form hexamers in phospholipid bilayers. *J. Mol. Biol.* 276:325–330.

Darst, S., M. Ahlers, P. Meller, E. Kubalek, R. Blankenburg, H. Ribi, H. Ringsdorf, and R. Kornberg. 1991. Two-dimensional crystals of streptavidin on biotinylated macromolecules. *Biophys. J.* 59:387–396.

DeGuzman, R. N., Z. R. Wu, C. C. Stalling, L. Pappalardo, P. N. Borer, and M. F. Summers. 1998. Structure of the HIV-1 nucleocapsid protein bound to the SL3 Psi-RNA recognition element. *Science.* 279:384–388.

Dememe, H., N. Jullian, N. Morellet, H. DeRocquigny, F. Cornille, B. Maigret, and B. P. Roques. 1994. Three-dimensional ^{1}H NMR structure of the nucleocapsid protein Ncp10 of Moloney murine leukemia virus. *J. Biomol. NMR.* 4:153–170.

Egger, M., F. Ohnesorge, A. L. Weisenhorn, S. P. Heyn, B. Drake, C. B. Prater, S. A. C. Gould, P. K. Hansma, and H. E. Gaub. 1990. Wet lipid-protein membranes imaged at submolecular resolution by atomic force microscopy. *J. Struct. Biol.* 103:89–94.

Faecke, M., A. Janetzko, R. Shoeman, and H. Krausslich. 1993. A large deletion in the matrix domain of the human immunodeficiency virus gag gene redirects virus particle assembly from the plasma membrane to the endoplasmic reticulum. *J. Virol.* 67:4972–4980.

Fass, D., R. A. Davey, C. A. Hamson, P. S. Kim, J. M. Cunningham, and J. M. Berger. 1997. Structure of a murine leukemia virus receptor-binding glycoprotein at 2.0 angstrom resolution. *Science*. 277: 1662–1666.

Fotiadis, D., D. Muller, G. Tsiotis, L. Hasler, P. Tittman, T. Mini, P. Jeno, H. Gross, and A. Engel. 1998. Surface analysis of the photosystem I complex by electron and atomic force microscopy. *J. Mol. Biol.* 283: 83–94.

Frank, J., M. Radermacher, T. Wagenknecht, and A. Verschoor. 1988. Studying ribosome structure by electon microscopy and computer-image processing. *Methods Enzymol.* 164:3–35.

Fuller, S. D., T. Wilk, B. E. Gowen, and H.-G. Krausslich. 1997. Cryo-electron microscopy reveals ordered domains in the immature HIV particle. *Curr. Biol.* 7:729–738.

Gamble, T. R., F. F. Vajdos, S. Yoo, D. Worthylake, M. Houseweart, W. I. Sundquist, and C. P. Hill. 1996. Crystal structure of human cyclophilin A bound to the amino-terminal domain of HIV-1 capsid. *Cell.* 87: 1285–1294.

Gamble, T. R., S. Yoo, F. Vajdos, U. von Schwedler, D. Worthylake, H. Wang, J. McCutcheon, W. Sundquist, and C. Hill. 1997. Structure of the carboxyl-terminal dimerization domain of the HIV-1 capsid protein. *Science.* 278:849–853.

Gitti, R. K., B. M. Lee, J. Walker, M. F. Summers, S. Yoo, and W. I. Sundquist. 1996. Structure of the amino-terminal core domain of the HIV-1 capsid protein. *Science.* 273:231–235.

Gross, I., H. Hohenberg, C. Huckhagel, and H.-G. Kräusslich. 1998. N-terminal extension of human immunodeficiency virus capsid protein converts the in vitro assembly phenotype from tubular to spherical particles. *J. Virol.* 72:4798–4810.

Hansen, M., and E. Barklis. 1995. Structural interactions between retroviral Gag proteins examined by cysteine crosslinking. *J. Virol*. 69: 1150–1159.

Hansen M., L. Jelinek, R. Jones, J. Stegeman-Olsen, and E. Barklis. 1993. Assembly and composition of intracellular particles formed by Moloney murine leukemia virus. *J. Virol.* 67:5163–5174.

Hansma, H. G., and J. H. Hoh. 1994. Biomolecular imaging with the atomic force microscope. *Annu. Rev. Biophys. Biomol. Struct.* 23: 115–139.

Henderson, R., J. Baldwin, T. Ceska, F. Zemlin, E. Beckmann, and K. Downing. 1990. Model for the structure of bacteriorhodopsin based on high-resolution electon cryo-microscopy. *J. Mol. Biol.* 213:899–929.

Hill, C., D. Worthylake, D. P. Bancroft, A. M. Christensen, and W. I. Sundquist. 1996. Crystal structures of the trimeric human immunodeficiency virus type 1 matrix protein: implications for membrane association and assembly. Proc. Natl. Acad. Sci. USA. 93:3099–3104.

Mingotaud, A.-F., C. Mingotaud, and L. K. Patterson. 1993. Handbook of Monolayers, Vol. 1. Academic Press, San Diego. 786–862.

Mou, J., J. Yang, C. Huang, and Z. Shao. 1994. Alcohol induces interdigitated domains in unilamellar phosphatidylcholine bilayers. *Biochemistry.* 33:9981–9985.

Mou, J., J. Yang, and Z. Shao. 1995. Atomic force microscopy of cholera toxin B-oligomers bound to bilayers of biologically relevant lipids. *J. Mol. Biol.* 248:507–512.

Muller, D. J., F. A. Schabert, G. Bundt, and A. Engel. 1995. Imaging purple membranes in aqueous solutions at sub-nanometer resolution by atomic force microscopy. *Biophys. J.* 68:1681–1686.

Nermut, M., D. Hockley, J. Jowett, I. Jones, M. Garreau, and M. Thomas. 1994. Fullerene-like organization of HIV Gag protein shell in virus-like particles produced by recombinant baculovirus. *Virology*. 198:288–296.

Rein, A., M. R. McClure, N. R. Rice, R. B. Luftig, and A. M. Schultz. 1986. Myristylation site in Pr65gag is essential for virus particle formation by Moloney murine leukemia virus. *Proc. Natl. Acad. Sci. USA.* 83:7246–7250.

Sackmann, E. 1983. Physical foundations of the molecular organization and dynamics of membranes. *In* Biophysics. Walter Hoppe, Wolfgang Lohmann, and Hubert Zeigler, editors. Springer-Verlag, New York. 425–457.

Sato, C., M. Sato, A. Iwasaki, T. Doi, and A. Engel. 1998. The sodium channel has four domains surrounding a central pore. *J. Struct. Biol.* 121:314–325.

Schmid, M., R. Dargahi, and M. Tam. 1993. SPECTRA: a system for processing electron images of crystals. *Ultramicroscopy.* 48:251–264.

Schmitt, L., C. Dietrich, and R. Tampe. 1994. Synthesis and characterization of chelator-lipids for reversible immobilization of engineered proteins at self-assembled lipid interfaces. *J. Am. Chem. Soc.* 116: 8484–8491.

Shao, Z., and J. Yang. 1995. Progress in high resolution atomic force microscopy in biology. *Q. Rev. Biophys.* 28:195–251.

Simon, S. A., and T. J. McIntosh. 1984. Interdigitated hydrocarbon chain packing causes the biphasic transition behavior in lipid/alcohol suspensions. *Biochim. Biophys. Acta.* 773:169–172.

Tauskela, J. S., M. Aklier, and M. Thompson. 1992. The size dependence of cholate-dialyzed vesicles on phosphatidylcholine concentration. *Anal. Biochem.* 201:282–287.

Unwin, P. N. T., and R. Henderson. 1975. Molecular structure determination by electron microscopy of unstained crystalline specimens. *J. Mol. Biol.* 94:425–440.

Uzgiris, E., and R. Kornberg. 1983. Two-dimensional crystallization technique for imaging macromolecules with application to antigen-antibody-complement complexes. *Nature.* 301:125–129.

Von Schwedler, U. K., T. L. Stemmler, V. Y. Klishko, S. Li, K. H. Albertine, D. R. Davis, and W. I. Sundquist. 1998. Proteolytic refolding of the HIV-1 capsid amino-terminus facilitates viral core assembly. *EMBO J.* 17:1555–1568.

Wang, C., Y. Zhang, J. McDermott, and E. Barklis. 1993. Conditional infectivity of a human immunodeficiency virus matrix domain deletion mutant. *J. Virol.* 67:8850–5561.

Wills, J., R. Craven, R. Weldon, T. Nelle, and C. Erdie. 1994. An assembly domain of the Rous sarcoma virus Gag protein required late in budding. *J. Virol.* 68:6605–6618.

Yeager, M., E. M. Wilson-Kubalek, S. G. Weiner, P. O. Brown, and A. Rein. 1998. Supramolecular organization of immature and mature murine leukemia virus revealed by electon cryo-microscopy: implication for retroviral assembly mechanisms. *Proc. Natl. Acad. Sci. USA.* 95: 7299–7304.

Zhang, Y., and E. Barklis. 1995. Nucleocapsid protein effects on the specificity of retrovirus RNA encapsidation. *J. Virol.* 69:5716–5722.